batteries

MDPI

Article

Rapid Estimation for the Maximum Remaining Capacity of Retired Lithium-Ion Batteries Based on CNN-CBAM-LSTM

Aqing Li [1], Penghao Cui [1], Yifei Cao [1,2,*], Peng Zhou [2], Lei Yang [3], Guochen Bian [4] and Zhendong Shao [5]

[1] Key Laboratory of Advanced Perception and Intelligent Control of High-End Equipment, Ministry of Education, Anhui Polytechnic University, Wuhu 241000, China
[2] School of Electrical Engineering, Anhui Polytechnic University, Wuhu 241000, China
[3] School of Computer and Information, Anhui Polytechnic University, Wuhu 241000, China
[4] Anhui Green Energy Technology Institute Co., Ltd., Hefei 230061, China
[5] Anhui Lvwo Energy Technology Co., Ltd., Lu'an 230061, China
* Correspondence: yfcao@ahpu.edu.cn

Abstract

With the continuous increase in the number of Retired Lithium-Ion Batteries (RLBs), accurately estimating their Maximum Remaining Capacity (MRC) has become a key challenge for rapid sorting and secondary utilization. Conventional detection methods often suffer from low efficiency and limited scalability for large-scale applications. To address these issues, this paper presents a rapid MRC estimation method using a hybrid Convolutional Neural Network (CNN), Conv Block Attention Module (CBAM), and Long Short-Term Memory (LSTM) architecture. The proposed approach extracts key voltage and capacity features from only the initial 30 min charging phase, integrating both factory and laboratory data. Specifically, the CNN captures local temporal patterns, the LSTM models long-term dependencies, and the CBAM adaptively emphasizes critical characteristics. Experimental results demonstrate that the proposed method significantly outperforms traditional approaches, achieving a testing R^2 of 98.05% and a Mean Absolute Percentage Error (MAPE) of 1.60%. These results highlight the superior performance of the proposed framework, exhibiting strong potential for high-throughput battery sorting and large-scale health monitoring systems.

Keywords: Retired Lithium-Ion Batteries; Maximum Remaining Capacity; Rapid Estimation; CNN-CBAM-LSTM

Check for updates

Academic Editor: Johan E. ten Elshof

Received: 15 February 2026
Revised: 15 April 2026
Accepted: 17 April 2026
Published: 20 April 2026

Copyright: © 2026 by the authors. Licensee MDPI, Basel, Switzerland. This article is an open access article distributed under the terms and conditions of the Creative Commons Attribution (CC BY) license.

1. Introduction

The rapid global adoption of new energy vehicles has precipitated a sharp increase in Retired Lithium-Ion Batteries (RLBs), making efficient and accurate assessment of their Maximum Remaining Capacity (MRC) a critical challenge for sustainable recycling and cascade utilization. China's retired power battery volume exceeded 40 GWh in 2023 and has surpassed 100 GWh in 2025. Batteries are typically retired when capacity degrades below 80% of the nominal value, yet they often retain sufficient MRC for secondary applications. Accurate MRC estimation is therefore essential to maximize resource efficiency. However, the current industrial standard, which need full charge–discharge cycle testing, requires up to 10 h per battery, rendering it impractical for large-scale screening. Furthermore, prevalent MRC estimation methods predominantly rely on stable, long-term data from new batteries, which fails to address the complex and highly heterogeneous MRC distribution characteristic of retired battery populations.

Existing estimation techniques face significant limitations in this context. Model-based approaches, such as Electrochemical Impedance Spectroscopy (EIS), offer high accuracy but demand specialized instrumentation and strict laboratory conditions [1,2]. Incremental Capacity (IC) analysis is more accessible but remains highly sensitive to measurement noise and operational variability, limiting its robustness in real-world sorting scenarios [3,4]. While data-driven machine learning methods reduce dependency on physical models, they often require manually engineered features and extensive, full life-cycle training data [5]. Recent deep learning advancements, particularly Convolutional Neural Networks (CNNs), automate feature extraction from partial charging data [6,7], and their integration with Long Short-Term Memory (LSTM) networks improves temporal modeling [8]. Attention mechanisms, such as the Convolutional Block Attention Module (CBAM), further enhance model focus on discriminative segments of the input data [9].

In parallel with the development of CNN and LSTM architectures, recent advances in sequence-to-sequence learning have introduced self-attention mechanisms and Transformer-based models to battery health prognostics. For instance, Ardakani et al. [10] developed a dynamic NARX Transformer to leverage multi-cycle data for long-term SOH estimation, demonstrating superior capability in capturing long-range dependencies. Similarly, Hou et al. [11] proposed an enhanced Transformer model constrained by physical information to jointly predict SOH and remaining useful life, while Zhang et al. [12] utilized multi-feature extraction combined with an improved Transformer for multi-step health prediction. Furthermore, to accommodate the high-throughput demands of industrial cascade utilization, there is a growing trend toward using partial charging segments rather than full-cycle data. Chen et al. [13] proposed a self-attention knowledge domain adaptation network to accurately estimate the state of health under shallow-cycle conditions, demonstrating the effectiveness of attention mechanisms in extracting degradation features from unlabeled partial charging curves.

Despite these promising developments, generalized Transformer models often introduce significant computational overhead and parameter redundancy when applied to short, fixed-length trajectories. This high algorithmic complexity restricts their direct deployment in resource-constrained, real-time industrial sorting systems where rapid inference is critical [14]. Therefore, developing a lightweight yet highly sensitive hybrid network that seamlessly balances advanced feature extraction capability with computational efficiency remains a pressing need for the large-scale screening of retired batteries.

To address the critical need for a rapid, accurate, and generalizable solution tailored to the high variability of industrial-scale retired batteries, this paper proposes a novel MRC estimation framework requiring only the first 30 min of charging data.

2. Methodology

2.1. Data Acquisition

The existing public data set is mainly for the aging test of new batteries in the laboratory environment, such as the NASA PCoE datasets, the Oxford Battery Degradation Dataset, and various CALCE and EV-aging datasets [15,16], which are widely used for battery modeling and prognostics. These datasets provide valuable cycle-life, relaxation, and EIS measurements, but they rarely cover large, heterogeneous populations of retired power batteries with complex first-life usage histories. However, these datasets lack the real-world diversity of retired batteries, often leading to decreased prediction accuracy during rapid industrial detection [17,18]. The samples used in this paper are all from the retired Lithium batteries recovered in the factory. Through the joint experiment of the factory and the laboratory, the charge–discharge cycle data of 1648 retired batteries of the same type are collected, the cycle test steps are shown in Figure 1.

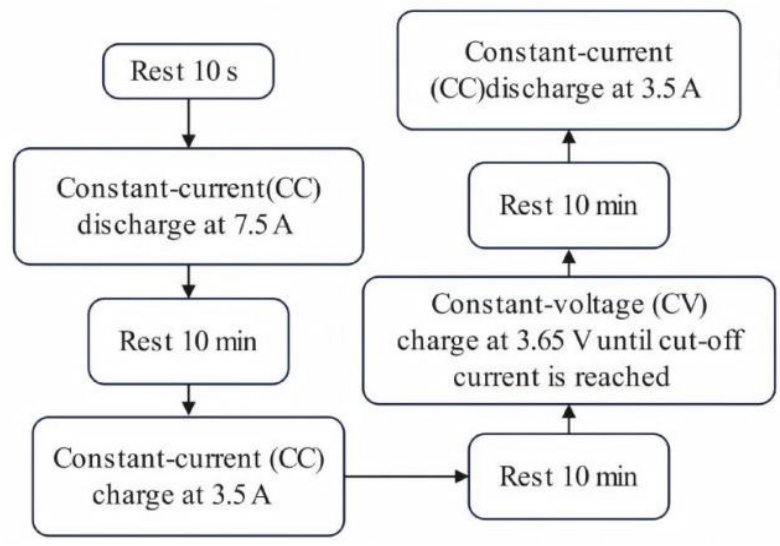


Figure 1. Schematic diagram of the RLBs charge–discharge setup and testing procedure.

It is important to note that to minimize the impact of environmental thermal fluctuations on battery polarization, all charging and discharging tests were conducted using professional battery testing equipment in air-conditioned environments [19]. The ground-truth MRC of each battery was determined by measuring the total discharged capacity during the standard constant-current (CC) discharge step at 3.5 A. The basic information on Lithium batteries is shown in Table 1.

Table 1. Parameters of RLBs.

Battery (Parameters)	Specifications (Value)	Battery (Parameters)	Specifications (Value)
Material	$LiFePO_4$	Dimensions	Φ32 mm × 80 mm
Rated Energy	24 Wh	Rated Capacity	7500 mAh
Nominal Voltage	3.2 V	Charge Cut-off Voltage	3.65 V
Charge Cut-off Current	0.225 A	Discharge Cut-off Voltage	2 V

Figure 2 presents the integrated distribution of charge–discharge data for retired Lithium batteries across three maximum remaining capacity intervals: 70–80%, 80–90%, and 90–100%. The data characteristics differ markedly among these ranges.

The MRC in 90–100% region, samples are the most abundant, with dense and well-defined voltage-capacity profiles that closely resemble those of fresh cells due to mild degradation; consequently, model predictions in this region tend to yield the smallest errors. The MRC in 80–90% range exhibits uniform data distribution and stable curve shapes, reflecting good capacity retention and consistency, thereby providing a reliable reference for modeling mid-capacity cells. In contrast, The MRC in 70–80% interval, which is a critical threshold for cascade utilization, shows originally sparse and scattered data owing to limited field-collected samples. To address this gap, laboratory multi-channel test data were introduced to supplement this interval, significantly increasing its sample density. This targeted augmentation results in a more balanced dataset across the full 70–100% MRC span, offering robust support for the training and validation of the proposed MRC prediction model, particularly in the low-MRC regime.

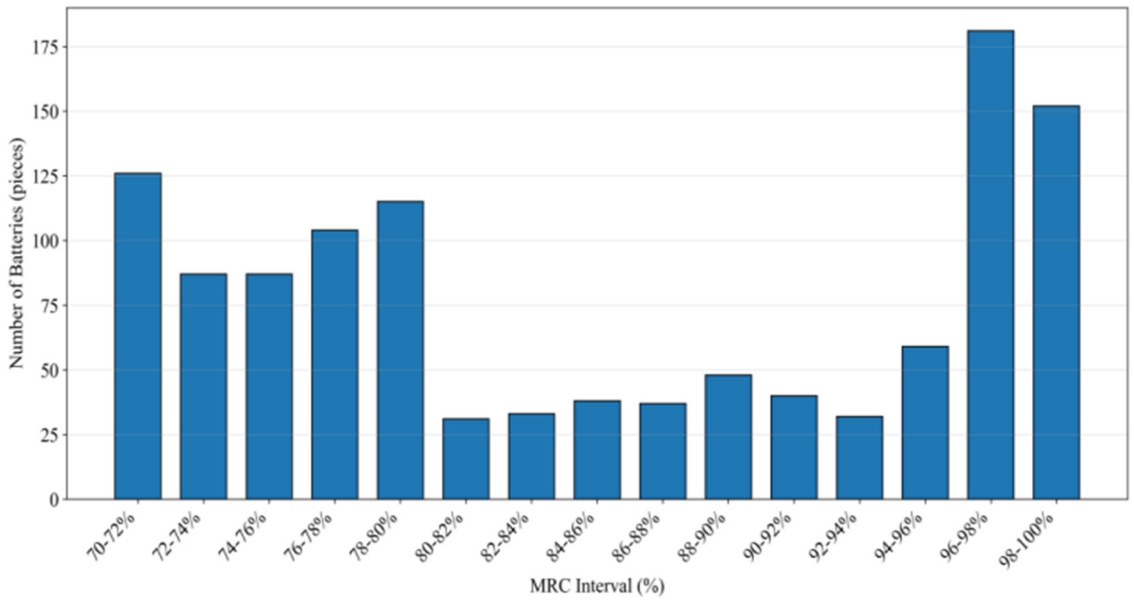


Figure 2. Charge–discharge data distribution of Lithium batteries with 70–100% MRC.

2.2. Characteristic Analysis of Retired Lithium-Ion Battery

During the lifetime of a Lithium battery, the decrease in MRC serves as a direct measure of performance degradation. As the MRC declines, parameters describing battery performance and stability not only shift in magnitude but also show growing dispersion across cells with identical nominal MRC. In experimental tests, the CC charging/discharging duration, together with the applied current, directly indicates usable capacity. Upon aging, the capacity-change rate in the voltage-plateau region varies significantly: heightened internal polarization, loss of active material lowering the plateau onset voltage, and shortened plateau duration collectively reduce the rate of capacity change. These dynamics are closely linked to the evolution of IC and dQ/dV curves, which are widely adopted as degradation indicators in IC-based analysis approaches.

Figure 3 presents dQ/dV curves for batteries across different MRC ranges. As MRC declines, both the capacity-change rate and the characteristic peaks within the voltage plateau exhibit marked evolution. Batteries with higher MRC display smooth, concentrated dQ/dV peaks, reflecting uniform electrochemical reactions and low polarization. At medium-low MRC levels, the curves become fluctuant with reduced reaction activity and increased polarization. Further degradation into the severe-aging range results in pronounced peak distortion and nonlinear jumps, indicating substantial active-material loss and elevated interfacial impedance. Consequently, the progression of dQ/dV peak position and magnitude provides a critical signature for characterizing and predicting battery MRC.

Figure 4a,b depict the charging process under full-voltage and partial-voltage conditions, respectively. The full-voltage charging cycle exhibits a clear dQ/dV-V peak with distinct characteristics along the complete curve. As the MRC declines, the effective charging current varies notably: low-MRC batteries demonstrate lower effective current and increased profile distortion, whereas high-MRC counterparts sustain higher and more stable current, reflecting superior charging performance and current-carrying capability.

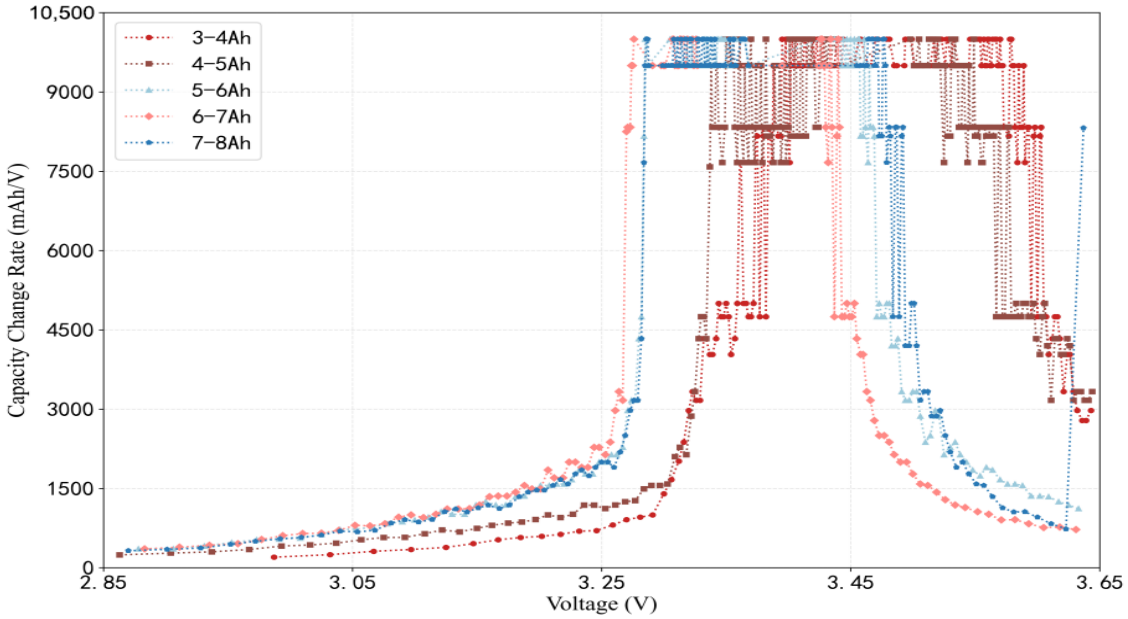


Figure 3. Comparison of incremental capacity-change rates under different states of health.

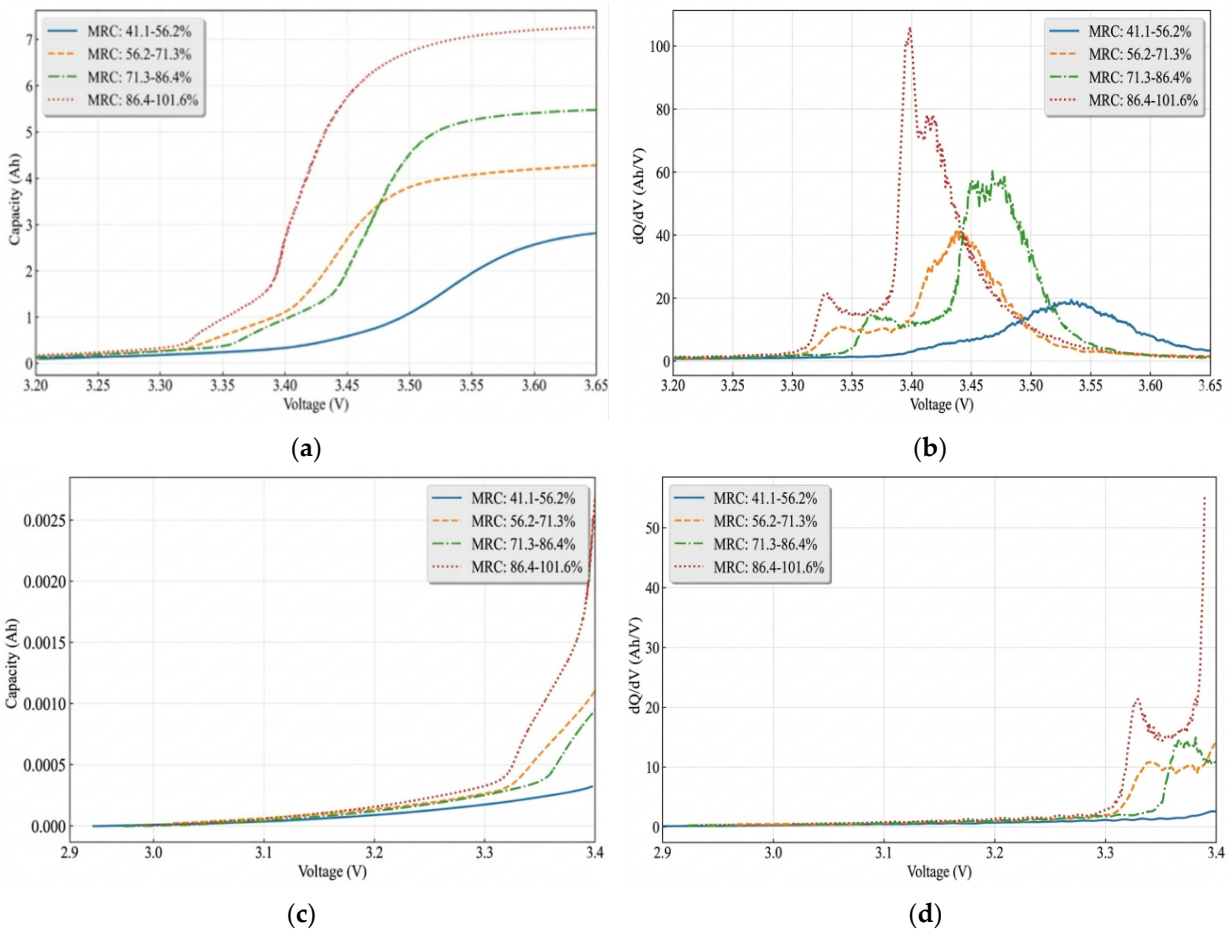


Figure 4. (**a**) Capacity–voltage curves of full CC-CV; (**b**) dQ/dV-V curves of full CC-CV; (**c**) capacity–voltage curves of partial CC-CV; (**d**) dQ/dV-V curves of partial CC-CV.

Figure 4c,d show the variation in the capacity increment (dQ/dV) with voltage for high- and low-MRC batteries. For high-MRC batteries, the incremental-capacity curve is relatively smooth, indicating a stable charging process and good electrochemical uniformity. In contrast, for low-MRC batteries, the dQ/dV curve becomes steeper and more irregular,

reflecting instability in the charging process and increased heterogeneity. Although the complete charging curve contains the full set of IC peaks, many peak characteristics are already visible within partial segments of the charging process. This observation suggests that it is feasible to use partial charging curves for model training and prediction, which can effectively extract key features for MRC assessment while avoiding the computational and data-processing burden associated with full-cycle curves.

2.3. Data Preprocessing

To standardize the input for the neural network and extract thermodynamically relevant features, the 30 min constant-current charging data (originally recorded at a sampling interval of 30 s) was transformed into 31 discrete voltage-capacity (V-Q) pairs using a voltage-driven interpolation strategy. Instead of relying on equal-time sampling, the voltage range observed within the first 30 min of charging was divided into 30 equal voltage intervals, yielding 31 fixed voltage nodes. The corresponding capacity at each exact voltage node was then accurately estimated using data interpolation.

This voltage-based interpolation approach offers significant advantages and directly addresses the challenge of capturing degradation characteristics from low-resolution data. First, battery aging mechanisms manifest as electrochemical phase transitions that occur at specific potential thresholds. By anchoring the data points to fixed voltage intervals rather than time, the extracted V-Q pairs naturally align with these thermodynamic potentials, inherently preserving the core information required for IC analysis. Second, raw industrial data sampled every 30 s often contains temporal measurement noise. Interpolating the data into 31 voltage-anchored points acts as an effective physical smoothing filter, eliminating high-frequency fluctuations that typically distort dQ/dV peak identification. Empirical validations confirm that this 31-point voltage-driven sequence strikes an optimal balance: it provides sufficient resolution to capture the macroscopic morphological deformations of the charging curve (reflecting polarization increments and capacity fade) while strictly compressing the input dimensionality to ensure ultra-fast, seconds-level inference for large-scale industrial sorting.

3. Models and Methods

The input to the model consists of voltage and capacity data within the partial-voltage window of 3.1 V–3.4 V. As depicted in Figure 5, these data are processed by two cascaded 1D convolutional layers for hierarchical feature abstraction. The first convolutional layer extracts local patterns from the voltage-capacity trajectories, with particular emphasis on dQ/dV characteristics that implicitly reflect changes in MRC and underlying electrochemical behavior. Since capacity increment evolves with aging, polarization, and state-of-charge (SOC) conditions, it is prioritized during feature learning [7]. Voltage features capture local variations such as rapid rises, quasi-constant plateaus, and minor fluctuations, whereas capacity-related features focus on the dynamic evolution of dQ/dV, especially shifts in peak shape and position across MRC levels. Features of dQ/dV are assigned higher weighting, enabling more accurate representation of aging- and polarization-induced capacity changes.

Following the feature extraction stage, a CBAM [9] is integrated to refine the learned representations. As illustrated in Figure 6, CBAM operates sequentially along the channel and spatial dimensions to enhance informative patterns and suppress redundant or less relevant features. Channel attention dynamically recalibrates feature maps by emphasizing channels most relevant to MRC estimation, while spatial attention aggregates contextual information and captures long-range dependencies across the sequential voltage-capacity data. This dual-attention mechanism enables the model to focus adaptively on critical

regions and feature channels, which are particularly the dominant capacity-increment characteristics, thereby strengthening the representation of higher-order patterns related to aging modes, polarization effects, and transition-zone dynamics. The refined features offer improved discriminability and robustness for subsequent health assessment and capacity estimation.

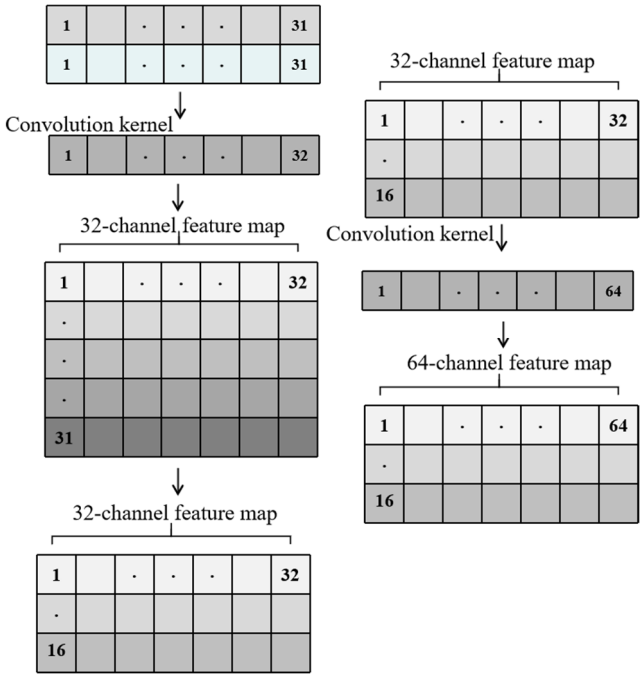


Figure 5. Convolutional feature extraction and transformation process of the CNN.

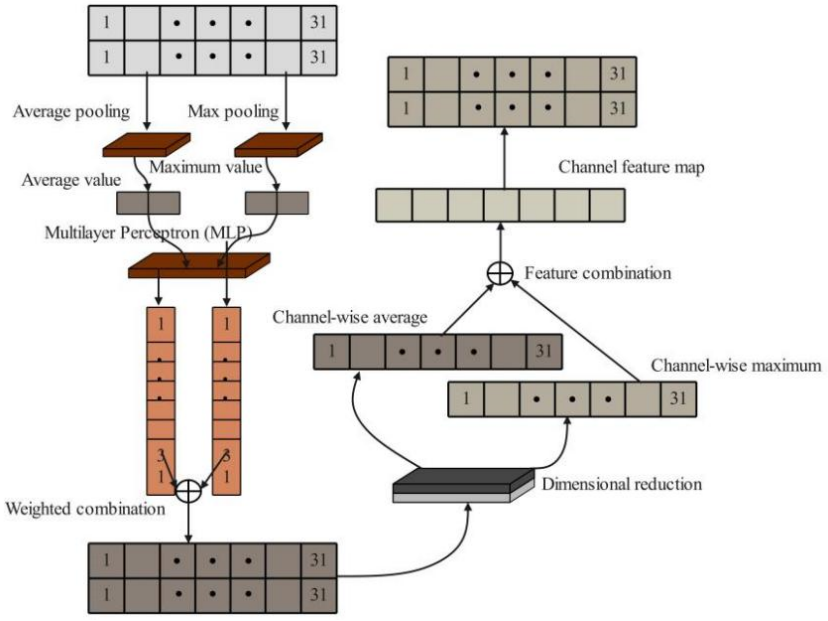


Figure 6. Structure and feature transformation process of the CBAM attention module.

The CBAM sequentially infers attention maps along the channel and spatial dimensions. By computing global average and max pooling, it generates robust channel attention weights, which are then complemented by spatial attention derived from inter-channel pooling operations. This dual mechanism effectively highlights key degradation features, such as incremental capacity peaks, while suppressing irrelevant background noise.

The proposed deep learning framework employs a CNN-LSTM-CBAM architecture to reconstruct the complete charging capacity curve and estimate the MRC from partial-voltage-capacity data. As shown in Figure 7, the model follows a structured three-stage pipeline: local feature extraction, temporal dependency modeling, and attention-based feature enhancement, collectively enabling accurate characterization of battery charging behavior.

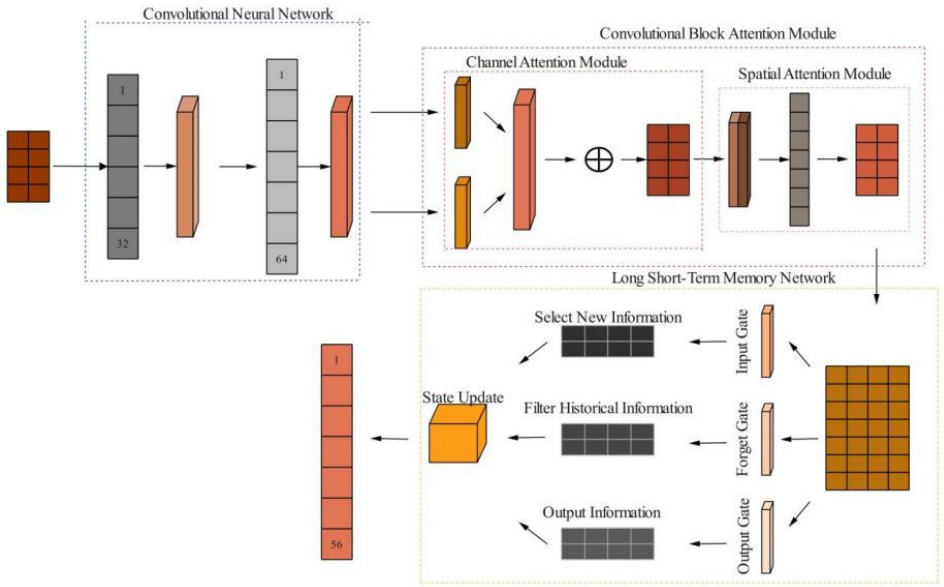


Figure 7. Overall structural framework of the CNN-LSTM-CBAM hybrid model.

The proposed hybrid network architecture takes 31 voltage–capacity (V-Q) pairs sampled from the initial charging segment as input, and outputs a sequence of 56 capacity points representing the reconstructed full charging profile. The model consists of four cascaded modules: a 1D convolutional feature extractor, a channel-spatial attention block, a temporal modeling unit, and a regression layer.

First, a two-layer 1D-CNN is employed to extract local nonlinear features, including slope variations and inflection points, from the input sequence. Each convolutional layer is followed by batch normalization and a ReLU activation function. The resulting features are then refined by a CBAM, which sequentially applies channel attention and spatial attention to adaptively emphasize informative feature channels and salient temporal regions.

Subsequently, the attention-weighted features are passed through a two-layer LSTM network to capture long-range temporal dependencies in the V-Q evolution, thereby modeling the underlying electrochemical dynamics over the charging process. Finally, the LSTM outputs are projected through a fully connected layer to generate the 56-point capacity profile.

During training, the predicted curve is compared against the measured full charging profile to compute the loss.

4. Results

4.1. Experimental Setup and Hyperparameter Optimization

To fully exploit the representation capacity of the proposed CNN-LSTM-CBAM architecture and ensure reproducibility, an automated Bayesian optimization framework was employed to explore the hyperparameter space, minimizing the Huber loss on the validation set. During training, the maximum number of epochs was set to 2000 with an early stopping patience of 20, and a dynamic learning rate scheduler was applied.

The network parameters were updated using the Adam optimizer with a batch size of 32. Table 2 details the predefined search space and the optimal values identified by the algorithm. Notably, the automated search determined precise non-integer optimal values, demonstrating the rigorous calibration achieved through this optimization process. The architectural details and optimal hyperparameter settings for these baselines are summarized in Table 3.

Table 2. Hyperparameter Search Space and Optimal Values for the Proposed Model.

Hyperparameters	Search Space	Optimal Value
Optimizer	(Adam, RMSprop, SGD)	Adam
Loss function	(MSE, MAE, Huber)	Huber
Initial learning rate	Log-uniform (1×10^{-5}, 1×10^{-2})	4.12×10^{-4}
Batch size	(16, 32, 64, 128)	32
Dropout rate	Uniform (0.2, 0.6)	0.512
CNN filters (Conv1, Conv2, Conv3)	(3, 5, 7, 9)	5, 7, 5
CNN activation function	(relu, elu, gelu)	relu
CBAM reduction ratio	(4, 8, 16)	8
LSTM units	(32, 64, 128, 256)	64
Dense layer units	(128, 256, 384, 512)	384
Dense activation	(relu, selu, tanh)	selu

Table 3. Architectural and hyperparameter settings for the baseline models.

Model	Hyperparameter	Search Space	Optimal Value
SVR	Kernel Function	(Linear, Poly, RBF)	RBF
	Regularization (C)	Uniform (1, 100)	61.38
	Epsilon (ϵ)	Uniform (0.01, 0.5)	0.125
	Gamma (γ)	Log-uniform (1×10^{-3}, 1)	0.099
Transformer	Number of Layers	(1, 2, 4, 6)	1
	Attention Heads	(2, 4, 8, 16)	2
	Embedding Dim	(32, 64, 128)	64
	Feed-forward Dim	(64, 128, 256, 512)	256
	Dropout Rate	(0.1, 0.2, 0.3, 0.5)	0.1

4.2. Model Performance Evaluation

To evaluate the proposed CNN-LSTM-CBAM model, we use a dataset combining laboratory measurements and industrial capacity-sorting line data. The input consists of 31 voltage-capacity feature points, and the output is a reconstructed full charging curve with 56 capacity points. Model performance is compared against two baselines (CNN-CBAM and CNN-LSTM) under identical dataset splits and training configurations. Evaluation metrics include the coefficient of determination (R^2), Mean Absolute Error (MAE), and Mean Absolute Percentage Error (MAPE).

Table 4 summarizes the performance metrics of the proposed model and baselines. The CNN-LSTM-CBAM model significantly outperforms all others, achieving the highest testing R^2 (98.05%) and the lowest testing MAPE (1.60%). Traditional machine learning approaches like SVR struggled to capture complex nonlinear degradation dynamics, while the optimized Transformer baseline exhibited noticeable parameter redundancy and lacked the necessary local inductive biases for extremely short (31-point) trajectories, yielding a testing MAPE of 3.72%.

Table 4. Performance comparison of MRC prediction based on different models.

Models	Training Set			Testing Set		
	R^2 (%)	MAE (mAh)	MAPE (%)	R^2 (%)	MAE (mAh)	MAPE (%)
CNN	94.50	148.28	2.33	94.83	151.62	2.38
Transformer	94.02	173.20	3.29	91.59	200.30	3.72
SVR	95.57	154.60	2.97	93.23	186.80	3.53
CBAM-CNN	92.94	184.50	2.96	96.51	128.03	2.07
LSTM-CNN	96.50	125.10	2.02	92.79	188.94	3.01
LSTM-CBAM-CNN	99.42	96.48	1.55	98.05	98.78	1.60

Figure 8 shows a point-by-point comparison of the prediction results and ground truth for the four models (CNN, CNN-CBAM, CNN-LSTM and CNN-LSTM-CBAM) on a typical test sample. It is evident that the prediction curve of the CNN-LSTM-CBAM model best matches the actual curve, with the smallest deviation among all models. In contrast, the other models exhibit larger local errors, especially near the voltage-plateau regions, where capturing subtle capacity changes is more challenging.

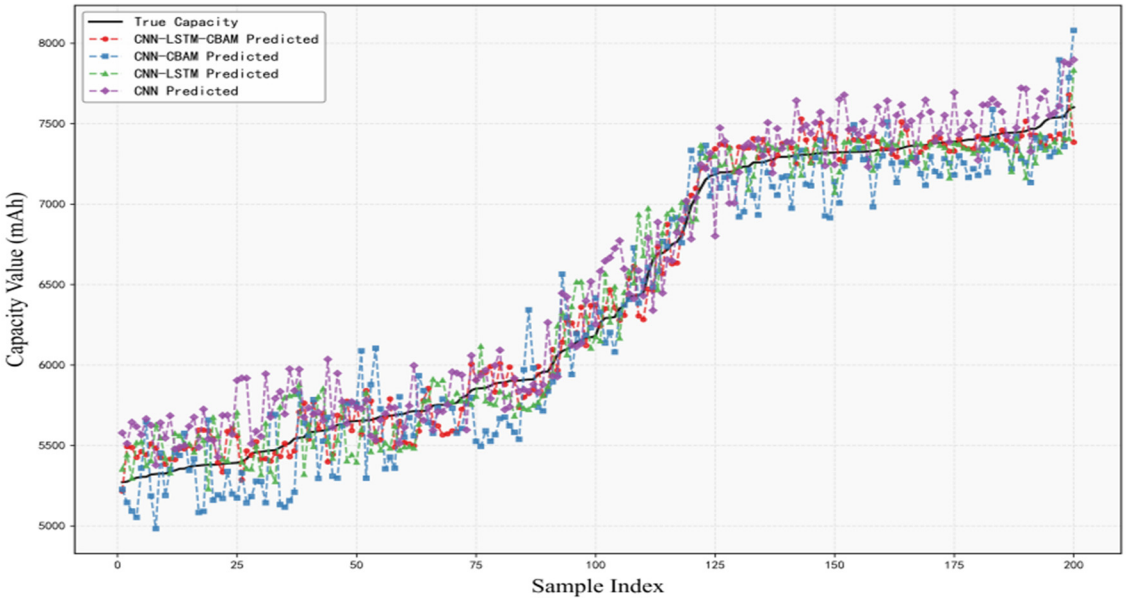


Figure 8. Comparison of predicted results and actual values for different models.

The CNN-LSTM-CBAM model exhibits the most accurate and stable performance. These results confirm that, by combining the temporal modeling capability of LSTM with the feature-enhancement capability of CBAM, the proposed CNN-LSTM-CBAM model can effectively capture nonlinear degradation behavior and sequence-dependent information in partial charging data. This leads to superior performance in MRC prediction compared with CNN-only and CNN-LSTM architectures, fully demonstrating the crucial role of the attention module in enhancing feature extraction and model accuracy.

Overall, the experimental results indicate that the proposed model not only achieves high fitting accuracy on the training data but also maintains low prediction errors on unseen test data. This performance is competitive with or superior to other deep-learning-based approaches reported in the literature for capacity and SOH estimation, especially considering that only partial charging data are used for prediction.

5. Discussion

The proposed CNN-LSTM-CBAM framework provides a highly efficient solution for the rapid SOH estimation of Retired Lithium-Ion Batteries. By utilizing only the initial 30 min charging data, this approach bypasses the time-consuming full charge–discharge cycles required by conventional methods. The model processed all 256 samples in 56.32 s, translating to an average comprehensive assessment time of approximately 7.25 s per cell. This ultra-low computational overhead confirms its capability for high-throughput, real-time sorting [20–23].

Despite the proposed model achieving good results, several limitations warrant future research. Currently, the proposed model is empirically validated on LFP batteries under controlled room temperatures. While the architecture's sensitivity to subtle dQ/dV features implies strong adaptability [24], direct application to other chemistries or environments with extreme thermal fluctuations may introduce prediction biases [25]. Future work will focus on introducing domain adaptation for diverse battery chemistries [26,27], enriching the dataset with extreme-aging samples, and incorporating ambient temperature as an explicit input feature to build a fully temperature-compensated health estimation framework.

In summary, the proposed framework successfully bridges the gap between rapid screening and accurate prediction, providing a scalable and efficient tool for industrial reuse assessment of retired batteries. Future work will focus on extending chemistry coverage, enriching data diversity, and exploring multimodal feature fusion to broaden applicability.

6. Conclusions

This paper proposes a rapid MRC estimation framework for retired Lithium batteries, based on a hybrid CNN-LSTM-CBAM architecture. The method addresses the low efficiency and long testing cycles of conventional full charge–discharge or specialized laboratory techniques by requiring only partial-voltage-capacity data from the initial charging phase. The architecture synergistically combines convolutional layers for spatial feature extraction, LSTM units for temporal dynamic modeling, and a CBAM attention mechanism to focus on discriminative curve intervals.

Experimental results demonstrate that the model achieves an average relative error below 2% under a 3.5 A discharge rate while reducing the per-battery detection time from several hours to within 30 min. This significant improvement in throughput highlights the method's strong potential for industrial sorting applications. The proposed approach provides a scalable and deployable solution for rapid residual capacity assessment, supporting more intelligent cascade utilization and accurate valuation of second-life batteries. Future work will extend the framework to diverse battery chemistries, enhance datasets with extreme-aging samples, and incorporate multimodal physical indicators to further improve robustness and generalization.

Author Contributions: A.L. has made contributions in methodology, experiments, initial draft writing, and editing. Y.C. has made contributions in conceptualization, methodology, initial draft reviewing, and revising. P.C. and L.Y. have made contributions to software, data organization, writing—review, and editing. P.Z. has made contributions to supervision, project management, funding acquisition, conceptualization, and methodology. G.B. and Z.S. have contributed to investigations, data management, and resources. All authors have read and agreed to the published version of the manuscript.

Funding: This work was supported by the Foundation of Science and Technology Research in Wuhu (2024kj018), and the Joint Opening Project of Anhui Engineering Research Center of Vehicle Display Integrated Systems and Joint Discipline Key Laboratory of Touch Display Materials and Devices in Anhui Province (VDIS and TDMD2024C02).

Data Availability Statement: The raw data supporting the conclusions of this article will be made available by the authors, without undue reservation.

Conflicts of Interest: Author Guochen Bian was employed by the company Anhui Green Energy Technology Institute Co., Ltd. Author Zhendong Shao was employed by the company Anhui Lvwo Energy Technology Co., Ltd. The remaining authors declare that the research was conducted in the absence of any commercial or financial relationships that could be construed as a potential conflict of interest.

References

1. Zhang, Y.; Tang, Q.; Zhang, Y.; Wang, J.; Stimming, U.; Alpha, A. Lee Identifying degradation patterns of lithium ion batteries from impedance spectroscopy using machine learning. *Nat. Commun.* **2020**, *11*, 1706. [CrossRef]
2. Liu, Y.; Wang, L.; Li, D.; Wang, K. State-of-health estimation of lithium-ion batteries based on electrochemical impedance spectroscopy: A review. *Prot. Control Mod. Power Syst.* **2023**, *8*, 39. [CrossRef]
3. Weng, C.; Cui, Y.; Sun, J.; Peng, H. On-board state of health monitoring of lithium-ion batteries using incremental capacity analysis with support vector regression. *IEEE Trans. Instrum. Meas.* **2013**, *235*, 36–44. [CrossRef]
4. Dubarry, M.; Anseán, D. Best practices for incremental capacity analysis. *Front. Energy Res.* **2022**, *10*, 1023555. [CrossRef]
5. Severson, K.A.; Attia, P.M.; Jin, N.; Perkins, N.; Jiang, B.; Yang, Z.; Chen, M.H.; Aykol, M.; Herring, P.K.; Fraggedakis, D.; et al. Data-driven prediction of battery cycle life before capacity degradation. *Nat. Energy* **2019**, *4*, 383–391. [CrossRef]
6. Shen, S.; Sadoughi, M.; Li, M.; Wang, Z.; Hu, C. Deep convolutional neural networks with ensemble learning and transfer learning for capacity estimation of lithium-ion batteries. *Appl. Energy* **2020**, *260*, 114296. [CrossRef]
7. Li, Y.; Li, K.; Liu, X.; Wang, Y.; Zhang, L. Lithium-ion battery capacity estimation—A pruned convolutional neural network approach assisted with transfer learning. *Appl. Energy* **2021**, *285*, 116410. [CrossRef]
8. Cao, Y.; Wang, R.; Li, Q.; Zhou, P.; Li, A.; Cui, P.; Tao, Q.; Shao, Z. Rapid Prediction of Maximum Remaining Capacity in Lithium-Ion Batteries Based on Charging Segment Features and GA_DBO_BPNN. *Batteries* **2025**, *10*, 375. [CrossRef]
9. Woo, S.; Park, J.; Lee, J.Y.; Kweon, I.S. CBAM: Convolutional Block Attention Module. In *Lecture Notes in Computer Science*; Springer: Cham, Switzerland, 2018; Volume 11211, pp. 3–19.
10. Ardakani, A.H.; Abdollahian, S.A.; Abdollahi, F. NARX Transformer: A Dynamic Model for Leveraging Multicycle Data in Long-Term Battery State of Health Estimation. *IEEE Trans. Instrum. Meas.* **2024**, *73*, 1–8. [CrossRef]
11. Hou, G.; Zhang, F.; Huang, C.; Huang, T. Joint prediction of SOH and RUL for Lithium-ion batteries by an enhanced Transformer model with physical information constraints. *Energy* **2025**, *336*, 138435. [CrossRef]
12. Zhang, Y.; Li, Z.; Kong, L.; Xu, H.; Shen, H.; Chen, M. Multi-step state of health prediction of lithium-ion batteries based on multi-feature extraction and improved Transformer. *J. Energy Storage* **2025**, *105*, 114622. [CrossRef]
13. Chen, X.; Qin, Y.; Zhao, W.; Yang, Q.; Cai, N.; Wu, K. A self-attention knowledge domain adaptation network for commercial lithium-ion batteries state-of-health estimation under shallow cycles. *J. Energy Storage* **2024**, *86*, 111197. [CrossRef]
14. Zhan, Y.; Yan, K.; Zheng, X. Integrating transformers into physics-informed neural networks: An approach to lithium-ion battery state-of-health prognostics. *Int. J. Electr. Power Energy Syst.* **2025**, *172*, 111173. [CrossRef]
15. Hassini, M.; Redondo-Iglesias, E.; Venet, P. Lithium-Ion Battery Data: From Production to Prediction. *Batteries* **2023**, *9*, 385. [CrossRef]
16. Saha, B.; Goebel, K. *Battery Data Set [DB/OL]*; NASA Ames Prognostics Data Repository: Moffett Field, CA, USA, 2007.
17. Birkl, C.A. *Oxford Battery Degradation Dataset 1 [DB/OL]*; University of Oxford Research Archive (ORA): Oxford, UK, 2017.
18. Calce. *Battery Research Data [DB/OL]*; Center for Advanced Life Cycle Engineering, University of Maryland: College Park, MD, USA, 2025.
19. Li, Z.; Qu, Z.; Jiang, Z.; Huang, H.; Tao, W. Degradation mechanism of lithium-ion battery under appropriate in-plane temperature gradient. *Green Energy Intell. Transp.* **2025**, *6*, 100352. [CrossRef]
20. Mowri, S.T.; Barai, A.; Sheikh, M.; Moharana, S.; Marco, J. Dataset for assessing the impact of first-life lithium-ion battery degradation on second-life performance. *Data Brief* **2025**, *63*, 112208. [CrossRef]
21. Fricke, K.A.; Nascimento, R.; Corbetta, M.; Kulkarni, C.; Viana, F. *An Accelerated Life Testing Dataset for Lithium-Ion Batteries with Constant and Variable Loading Conditions*; NASA Technical Report; National Aeronautics and Space Administration: Washington, DC, USA, 2023.
22. Zhu, J.; Mathews, I.; Ren, D.; Li, W.; Cogswell, D.; Xing, B.; Sedlatschek, T.; Kantareddy, S.N.R.; Yi, M.; Gao, T.; et al. End-of-life or second-life options for retired electric vehicle batteries. *Cell Rep. Phys. Sci.* **2021**, *2*, 100537. [CrossRef]
23. Song, H.; Zheng, C.; Wang, J. An overview about second-life battery utilization for energy storage systems. *Energies* **2024**, *17*, 6163. [CrossRef]

24. Kong, W.; Zhang, X.; Zhao, Y. Residual capacity estimation and consistency sorting of retired lithium batteries in cascade utilization process: A review. *Green Manuf. Oper.* **2025**, *3*, 1. [CrossRef]
25. Hasib, S.A.; Islam, S.; Chakrabortty, R.K.; Ryan, M.J.; Saha, D.K.; Ahamed, H.; Moyeen, S.I.; Das, S.K.; Ali, F.; Islam, R.; et al. A comprehensive review of available battery datasets, RUL prediction approaches, and advanced battery management. *IEEE Access* **2021**, *9*, 86166–86193. [CrossRef]
26. Stroebl, F.; Petersohn, R.; Schricker, B.; Schaeufl, F.; Bohlen, O.; Palm, H. A multi-stage lithium-ion battery aging dataset using various experimental design methodologies. *Sci. Data* **2024**, *11*, 1020. [CrossRef] [PubMed]
27. Pozzato, G.; Allam, A.; Onori, S. Lithium-ion battery aging dataset based on electric vehicle real-driving profiles. *Data Brief* **2022**, *41*, 107995. [CrossRef] [PubMed]

Disclaimer/Publisher's Note: The statements, opinions and data contained in all publications are solely those of the individual author(s) and contributor(s) and not of MDPI and/or the editor(s). MDPI and/or the editor(s) disclaim responsibility for any injury to people or property resulting from any ideas, methods, instructions or products referred to in the content.